UPLC-MS/MS-based metabolomic characterization and comparison of pancreatic adenocarcinoma tissues using formalin-fixed, paraffin-embedded and optimal cutting temperature-embedded materials

DI FENG[1*], JING YUAN[2*], QI LIU[3], LI LIU[4], XU ZHANG[1], YALI WU[1], YIFAN QIAN[1], LIPING CHEN[1], YAN SHI[5**] and MANCANG GU[1**]

[1]College of Pharmaceutical Sciences, Zhejiang Chinese Medical University, Hangzhou, Zhejiang 311402; [2]Department of Pathology, Chinese PLA General Hospital, Beijing 100853, P.R. China; [3]Department of Dermatology, Johns Hopkins University School of Medicine, Baltimore, MD 21231, USA; [4]Department of Epidemiology and Biostatistics, Ministry of Education Key Lab of Environment and Health, School of Public Health, Huazhong University of Science and Technology, Wuhan, Hubei 430030; [5]Department of Medical Oncology, Chinese PLA General Hospital, Beijing 100853, P.R. China

Received May 8, 2019; Accepted September 9, 2019

DOI: 10.3892/ijo.2019.4898

Abstract. The purpose of the present study was to compare metabolites from formalin-fixed and paraffin-embedded (FFPE) pancreatic tissue blocks with those identified in optimal cutting temperature (OCT)-embedded pancreatic tissue blocks. Thus, ultra-performance liquid chromatograph-mass spectrometry/mass spectrometry-based metabolic profiling was performed in paired frozen (n=13) and FFPE (n=13) human pancreatic adenocarcinoma tissue samples, in addition to their benign counterparts. A total of 206 metabolites were identified in both OCT-embedded and FFPE tissue samples. The method feasibility was confirmed through reproducibility and a consistency assessment. Partial least-squares discriminant analysis and heatmap analysis reliably distinguished tumor and normal tissue phenotypes. The expression of 10 compounds, including N-acetylaspartate and creatinine, was significantly different in both OCT-embedded and FFPE tumor samples. These ten compounds may be viable candidate biomarkers of malignant pancreatic tissues. The super-categories to which they belonged exhibited no significant differences between FFPE and OCT-embedded samples. Furthermore, purine, arginine and proline, and pyrimidine metabolism used a shared pathway found in both OCT-embedded and FFPE tissue samples. These results supported the notion that metabolomic data acquired from FFPE pancreatic cancer specimens are reliable for use in retrospective and clinical studies.

Correspondence to: Dr Yan Shi, Department of Medical Oncology, Chinese PLA General Hospital, 28 Fuxing Road, Beijing 100853, P.R. China
E-mail: shibaiwan12@vip.sina.com

Dr Mancang Gu, College of Pharmaceutical Sciences, Zhejiang Chinese Medical University, 4A119 Gaoke Road, Hangzhou, Zhejiang 311402, P.R. China
E-mail: gmancang@zcmu.edu.cn

*,**Contributed equally

Abbreviations: FC, fold change; FDR, false discovery rate; FFPE, formalin-fixed paraffin-embedded; HMDB, Human Metabolome Database; KEGG, Kyoto Encyclopedia of Genes and Genomes; *KRAS*, Kirsten rat sarcoma viral oncogene; MS, mass spectrometry; PDAC, pancreatic adenocarcinoma; PLS-DA, partial least-squares discriminant analysis; OCT, optimal cutting temperature; UPLC, ultra-performance liquid chromatography

Key words: clinical metabolic profiling, FFPE tissues, OCT-embedded tissues, pancreatic cancer, UPLC-MS, metabolic pathway enrichment analysis

Introduction

Pancreatic adenocarcinoma (PDAC) is a leading cause of cancer-related mortality in Western countries; most patients with PDAC are diagnosed with advanced disease and survive <12 months after diagnosis (1,2). Although surgery, neoadjuvant chemotherapy, radiation therapy and other treatments have been employed over previous decades, the overall survival rate of patients with PDAC has not improved markedly (3). Thus, patients with PDAC have a poor prognosis and high rates of mortality. Therefore, precision treatment of PDAC is important in increasing the survival rate and improving therapeutic options for different stages of PDAC.

Metabolomics has emerged as a field that elucidates pathological mechanisms (4), improves disease diagnosis (5), screens biomarkers (6,7) and provides improved assessments of the rationality of drugs (8). Additionally, metabolomics is downstream of other 'omics', such as genomics, transcriptomics and

proteomics, and analyzes biosynthetic and catabolic pathways involving multiple compounds, such as the cellular, tissue, biofluid and other physiological environments. Metabolomics can identify potential interactions between genes, enzymes, metabolic reactions or metabolic compounds; for example, glutamine metabolism can support pancreatic cancer growth via a *KRAS*-driven pathway (9,10). Therefore, metabolomics represents a powerful tool to profile tumors and identify precision treatment strategies (11,12).

PDAC tumors, like numerous tumors, exhibit altered metabolism in order to meet the needs of unconstrained proliferation (13). Abnormal energy utilization in cancer was first recognized by Warburg (14), who noted that cancer cells primarily rely on glycolysis followed by lactic acid fermentation for ATP production, despite the availability of oxygen. This process is commonly referred to as 'aerobic glycolysis' (15). In addition, other metabolic pathways, such as lipid or fatty acid metabolism, and amino acid metabolism, are found to be defective in PDAC (16). Hence, metabolon studies are important for PDAC research. The comparison of metabolic profiles between various types of pancreatic cancer may allow clinicians to detect an altered pancreatic profile at early stages, enabling early diagnosis of pancreatic cancer. Therefore, it is critical to identify PDAC biomarkers for further studies. Certain metabolites, such as leucine, isoleucine, valine, lactate, alanine, phosphocholine, glycerophosphocholine, taurine, betaine, taurine, creatine and glutamate, were reported to be potential biomarkers of PDAC in tissues (17,18). Furthermore, metabolic studies have revealed the pathogenesis of PDAC, allowing researchers to look for potential targets for drug therapy. For example, PDAC relies on increased utilization of glutamine to fuel anabolic processes (16). Drawing on the aforementioned knowledge, researchers have identified a non-canonical pathway of glutamine metabolism involving a *KRAS*-driven pathway, which is required for tumor growth (4).

However, the lack of well-annotated biological materials with long-term storage capability is a bottleneck in human tissue metabolomics research. At present, formalin-fixed paraffin-embedded (FFPE) materials are widely utilized in metabolomics and other 'omics' research (19). Due to the widespread availability and long-term stability of FFPE materials, accurately profiling the metabolite content of these tumor samples could assist in identifying biomarkers for clinical diagnosis.

There are three powerful analytical techniques applied for the assay and quantification of metabolites; liquid chromatography (LC) coupled with mass spectrometry (MS), gas chromatography coupled with MS and nuclear magnetic resonance (20). In addition, Fourier transform ion cyclotron resonance MS coupled to matrix-assisted laser desorption/ionization has also been utilized for metabolic analysis (19). Using this platform, the overlap of m/z species detected in FFPE samples was 72% compared with fresh frozen samples.

While there is literature on metabolomic profiling using FFPE materials in studies of sarcomas and prostate cancer, few publications have demonstrated the effect of metabolomic profiling from PDAC FFPE tissue samples (21,22). In the present study, optical cutting temperature (OCT)-embedded and FFPE human pancreatic cancer tissue samples were compared using ultra-performance (UP)LC-MS/MS-based metabolomics to explore the metabolites preserved in FFPE. Physical and chemical properties of the metabolites were also investigated. This study examined the method's feasibility through reproducibility and a consistency assessment. In addition, differential metabolites and pathways were explored to examine whether tissues were malignant or non-malignant.

Materials and methods

Human pancreatic tissue. A total of 13 patients with PDAC were selected in between July and September 2018 (age range, 41-71 years; mean age 60.0±7.3 years; gender, 7 male and 6 female). Demographic profiles of all patients are presented in Table I. Both tumor and normal OCT-embedded and FFPE tissues were extracted and processed from each patient at Chinese PLA General Hospital (Beijing, China). Samples were obtained during surgical resection. An OCT compound medium (Sakura Finetek USA, Inc.) containing 10.24% w/w polyvinyl alcohol, 4.26% w/w polyethylene glycol and 85.50% w/w of a nonreactive ingredient was used to create the blocks (23). The sample collection protocol was approved by the Institutional Review Board of the Chinese PLA General Hospital (permit no. S2018-041-01), and all subjects provided informed consent for inclusion in the study. The OCT-embedded and FFPE tissue sections were collected by the Department of Pathology at Chinese PLA General Hospital according to protocols as described previously (24). Tissue blocks were sectioned at 20 μm and stained with hematoxylin and eosin to delineate tumor and healthy areas in each block. In brief, the normal tissue specimen was taken from areas directly adjacent to the tumor areas. The FFPE tissue blocks were stained with hematoxylin for 10 min at room temperature and eosin for 30 sec at room temperature. After that each slide was dehydrated in ethanol (70-100%) for 12 min and 100% xylene for 3 min at room temperature, and was covered with a coverslip and mounting neutral balsam medium (Beijing Solarbio Science & Technology Co., Ltd.). Each tissue block was observed under an optical microscope (magnification, x100 and x400) and images of at least ten fields of view were captured.

Extraction of metabolites. Methanol (80%; 1 ml) was added directly to each OCT-embedded and FFPE tissue section and mixed thoroughly. Both types of tissue sample were then incubated at 70˚C for 45 min. All samples were placed on ice for 30 min and centrifuged for 15 min at 14,000 x g at 4˚C, and the supernatant was transferred into a new 1.5-m microcentrifuge tube. Centrifugation was repeated once under the same conditions. Finally, each supernatant was collected into a new microcentrifuge tube and stored at -80˚C.

Untargeted metabolite profiling. The metabolite profiling of both FFPE and OCT tissue samples were determined following protocols as previously reported (25). All methods involved utilized a Waters® ACQUITY I-CLASS UPLC (Waters Corporation) and AB SCIEX QTRAP 5500 high resolution/accurate mass spectrometer (SCIEX), which consisted of a heated electrospray ionization source and Orbitrap mass analyzer at 35,000 mass resolution. The temperature of column was to 30˚C, the flow rate was 300 μl/min and the sample

Table I. Clinical features of pancreatic adenocarcinoma cases.

Characteristic	Finding
Age (years)	60.0±7.3
Gender	
Male	7 (54)
Female	6 (46)
Cancer stage	
I	4 (32)
II	5 (38)
III	2 (15)
IV	2 (15)

Data are presented as mean ± SD or n (%).

injection volume was 2 μl. A series of internal standards at fixed concentrations was added to reconstituted sample solutions to ensure injection and chromatographic consistency. The resulting sample solution was divided into three parts: First, one aliquot was assessed using acidic positive ion-optimized conditions for hydrophilic compounds. The aliquot was gradient eluted from a C18 column (Waters ACQUITY UPLC® BEH C18-2.1x50 mm; 1.7 μm) using chormatographic grade methanol (purity >99.99%) and acetonitrile (purity >99.99%) as well as water phase containing 0.05% perfluoropentanoic acid and 0.05% formic acid. The gradient program was: 8% methanol, 4% acetonitrile and 88% water phase for 3 min, increased to 12% methanol, 6% acetonitrile and 82% water phase over 1 min and hold for 4 min. Then increased to 30% methanol, 15% acetonitrile and 55% water phase over 2 min and hold for 4 min, followed by increase to 50% methanol, 25% acetonitrile and 25% water phase over 3 min and hold for 5 min, and back to 8% methanol, 4% acetonitrile and 88% water phase over 1 min and hold for 3 min to re-equilibrate the column. Second, the second aliquot was analyzed using basic negative ion-optimized conditions using a separate dedicated C18 column. For each analysis, the sample was eluted from a gradient column using methanol and water containing 5 mM ammonium bicarbonate at pH 8. The gradient program was: 90% methanol for 1.5 min, decreased to 75% methanol over 1 min and hold for 3 min, decreased to 35% methanol over 3 min and hold for 3 min, then decreased to 10% methanol over 1.5 min and hold for 3 min, and back to 90% methanol over 1 min and hold for 5 min to re-equilibrate the column. Finally, the third aliquot was determined through negative ionization and gradient eluted from a hydrophilic interaction liquid chromatographic column (Waters ACQUITY UPLC® BEH Amide-2.1x50 mm; 1.7 μm) using acetonitrile and water with 8 mM ammonium formate at pH 10. The gradient program was: 85% methanol for 3 min, decreased to 40% methanol over 4.5 min and hold for 2 min, then decreased to 15% methanol over 3 min and hold for 5 min, and back to 85% methanol over 1 min and hold for 5 min to re-equilibrate. Nitrogen was used as the dry gas and the flow rate was 8 l/min, sheath gas temperature was 400˚C and the desolvation gas temperature was 350˚C; the nebulizer pressure was 15 psi. The mass spectrum of each sample was scanned between 70-1,000 m/z using dynamic exclusion according to methods. Raw data files were archived and extracted as described below.

Metabolite identification. MS raw data were pre-processed by MultiQuant 2.0 (SCIEX) as previously described (26). Compounds were identified in comparison to library entries of purified standards or recurrent unknown entities. Furthermore, biochemical properties of compounds were identified as follows: Retention time within a narrow retention time/index window of the proposed identified compound, and accurate sample MS data ±10 ppm match to the library and the MS/MS scores between the experimental mass spectra and authentic standards. The MS/MS forward and reverse scores were based on a comparison of the ions present in the experimental data to the ions' spectra present in the library. While similarities may be found among these molecules based on one of above factors, all those data points above can be utilized to distinguish different compounds. All identified metabolites were divided into eight super-classes (nucleotide, cofactors and vitamins, xenobiotics, amino acid, lipid, carbohydrate, energy and peptide) and consequently several sub-classes based on previous reports (27).

Statistical analysis. Detailed information regarding the categorization of metabolites detectable in FFPE and OCT-embedded samples (super-class and subclass), substituents (an atom or group of atoms taking the place of another atom group or occupying a specific position in a molecule) and chemical/physical properties can be obtained from the Human Metabolome Database (HMDB; http://www.hmdb.ca/) (28,29), Small Molecule Pathway Database (http://www.smpdb.ca), and Kyoto Encyclopedia of Genes and Genomes (KEGG; http://www.genome.jp/kegg).

The identified metabolite data were pre-processed prior to conducting further analysis. The raw peak intensity table was inputted into MetaboAnalyst 4.0 (http://www.metaboanalyst.ca), an online platform intended for metabolomic analysis (30,31). For multivariant analysis, the cutoff was set at 77% to ensure compounds that may be detected exclusively in one class were not excluded (FFPE or OCT-embedded). Otherwise, the missing values were input as half of the minimum positive value in the original data. Next, data filtering was performed; variables were removed if their relative standard deviation was >25%. For completeness sake, normalization was also conducted based on the median followed by $\log_2$ transformation and mean centering (mean-centered only). The resultant data were used for further analysis.

R software (version 3.5.1) was used for all statistical analyses (32). The Fisher exact test was used to evaluate the differences in a number of metabolites belonging to a specific category detected or non-detected in FFPE samples. Pearson correlation analysis was used to correlate metabolites between FFPE and OCT-embedded samples. Pairwise comparisons of physical/chemical properties of metabolites were performed according to the Mann-Whitney test. Benjamini-Hochberg false discovery rate (FDR) correction was used to adjust all P-values and reduce false-positive discovery for multiple testing (33). The q conversion algorithm was used to

calculate FDRs in multiple comparisons (33). The threshold for significance was FDR<0.05 for all tests.

To distinguish between normal and tumor groups in the OCT-embedded and FFPE samples, a partial least-squares discriminant analysis (PLS-DA) was performed. All compounds in heatmaps were ordered via hierarchical clustering (Ward linkage) implemented in the R package ggplot2 (32). Then, the 40 common metabolites with the most significant P-values as determined by Student's t-test were selected.

Volcano diagram analysis was performed in MetabolAnalyst 4.0 platform (http://www.metaboanalyst.ca), to identify metabolites presenting significant differences between the tumor and normal groups. P-values were calculated by Student's t-test, and the fold change (FC) of tumor/normal was calculated. The differential metabolites were identified by a P<0.05 and an FC>1.5.

Pathway analysis was also performed using the MetaboAnalyst 4.0 platform. First, HMBD IDs of the differential compounds between OCT-embedded and FFPE samples were inputted into the platform. The differential compounds were identified by Student's t-test; FC and HMDB IDs are available in the HMDB. The pathway library used for pathway analysis was 'Homo sapiens (human)'. Representation analysis was conducted using the hypergeometric test, and pathway topology analysis was conducted using the relative-betweenness centrality. If compounds involved within the pathway belonged to OCT-embedded and FFPE samples, the pathway would be defined as a shared pathway. In order to analyze a correlation network of the compounds in shared pathways, MetScape (34), an app implemented in Java and integrated with Cytoscape (version 3.2.1), was used (35). KEGG IDs, P-values and log2 FCs of selected compounds were inputted into the app, and Compound-Gene was selected to build a network. Once the core program was completed, the compound-gene network was created, and the node color was set based on the log2 FC of each metabolite.

Results

Human pancreatic tissue samples. OCT-embedded and FFPE tissue slices from 13 patients with pancreatic cancer were collected. Both tumor and normal OCT-embedded and FFPE tissue samples were collected from each patient during surgical resection. Patient details are summarized in Table I. FFPE samples were stained with H&E to identify the tumor and normal tissue areas in each block. Fig. S1 presents the distinction between tumor tissue and normal tissue, indicating that the tissue architecture was preserved and could be used for further analysis. As shown in the figure, tumor cells were severely atypia and the glands were irregular, which infiltrated in the desmoplastic stroma. However, the tissue in normal blocks presented without atypia.

Reproducibility and consistency assessment. After UPLC-MS/MS profiling, a total of 570 and 210 metabolites were identified in OCT-embedded and FFPE samples, respectively. However, a high rate of missing values caused difficulties for downstream analysis. To combat this issue, a rule to clear data for further analysis was generated, which excluded any metabolites absent from ≥77% of the raw data obtained from UPLC-MS/MS experiments. The remaining missing values were input as half of the minimum positive value in the original data. Then, a data filtering and normalization process was conducted. The specific protocol was presented in Fig. 1. Finally, a total of 206 metabolites passed the filtering criteria and were preserved in both FFPE and OCT-embedded samples; an additional 330 metabolites were detected only in frozen OCT-embedded samples, and 4 were found only in FFPE samples (Fig. 2A). The relative signal intensities of all shared metabolites found in OCT-embedded and FFPE samples are presented in Fig. 2B.

To assess data reproducibility in FFPE or OCT-embedded replicates, Pearson correlation analysis was conducted for the 206 shared metabolites in the 13 patients. As shown in Fig. 2C, the correction coefficients calculated in FFPE samples (normal vs. tumor) ranged between 0.844 and 0.864 (median value, 0.856), indicating little variability among samples and verifying the feasibility of the method. Similar to the results obtained with FFPE sample replicates, OCT-embedded sample replicates indicated high degree of reproducibility ranging between 0.884 and 0.900 (median value, 0.892; Fig. 2C).

The median of correlation coefficients between FFPE and OCT-embedded samples were 0.561 (ranging between 0.532 and 0.589) and 0.549 (ranging between 0.519 to 0.577) in normal and tumor groups, respectively (Fig. 2D).

The consistency in the seven metabolite super-classes between OCT-embedded and FFPE samples were presented in Fig. S2. The correlation coefficients were calculated for each metabolite super class, including nucleotide, cofactors and vitamins, xenobiotics, amino acid, lipid, carbohydrate and energy. The median value of the correction coefficients was >0.500, except for carbohydrate (r=0.380 in normal tissues and r=0.487 in tumor tissues) and cofactors and vitamins (r=0.258 in normal tissues and r=0.095 in tumor tissues).

Metabolites preserved in FFPE tissue samples. To examine the similarity of metabolomic data between FFPE and OCT-embedded tissues, the study focused on the 206 shared metabolites found in both types of samples, and the 330 only preserved in OCT-embedded samples. As shown in Fig. 2E, it was confirmed that only several classes of metabolites could be recovered in FFPE samples. The present study then compared the rate of detection in FFPE samples with the corresponding OCT-embedded samples according to the class of the metabolite. Using a Fisher exact test, the differences in detected or undetected FFPE samples were evaluated. The P-values and FDR are listed in Table SI. The metabolites belonging to nucleotide, cofactors and vitamins, xenobiotics, amino acid, lipid and carbohydrate super-classes presented no significant difference between FFPE and OCT-embedded samples (P>0.05), illustrating that the extent to which these metabolites were preserved in FFPE samples was similar to their OCT-embedded counterparts. Of note, 103 of 245 lipids were preserved in FFPE groups (42%; P=0.13; FDR=0.26). It was also found that metabolites in the lipid class had good detectability, such as sterol (33%; P>0.999; FDR=1.00) and lysolipid (41%; P=0.85; FDR=1.00). Conversely, no peptides were preserved in FFPE samples (0%; $P=5.46x10^{-7}$;

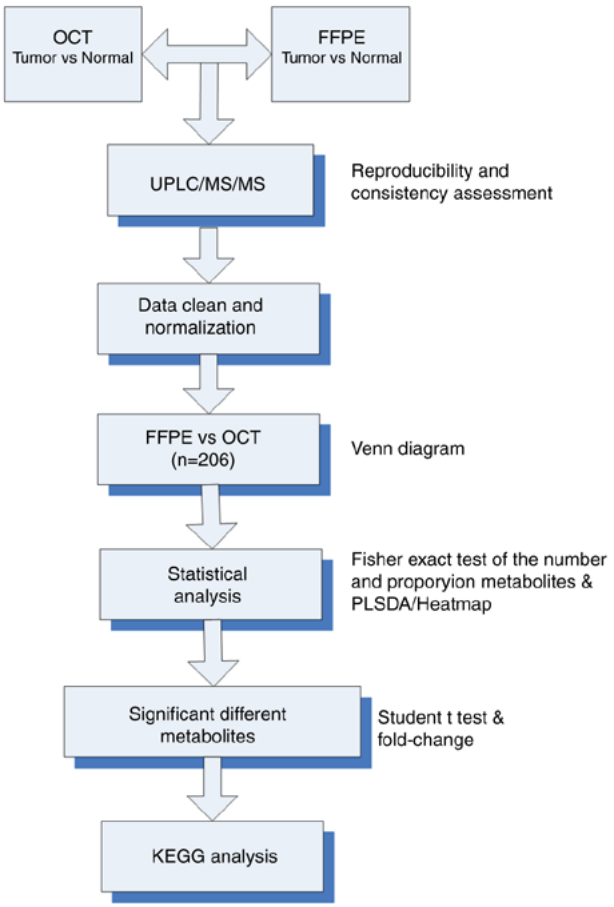

Figure 1. Schematic overview of the protocol used to analyze metabolite data in OCT-embedded and FFPE samples. FFPE, formalin-fixed paraffin-embedded; KEGG, Kyoto Encyclopedia of Genes and Genomes; OCT, optimal cutting temperature; UPLC-MS/MS, ultra-performance liquid chromatography-tandem mass spectrometry.

FDR=4.37x10^{-6}). In addition, metabolites in each sub-class were compared between OCT-embedded and FFPE groups, and certain similarities between the two groups were identified, including metabolites belonging to purine, adenine, pyrimidine, orotate, urea, arginine and proline metabolism subclasses (all FDR>0.05). Meanwhile, the differences between the chemical/physical properties were evaluated using the non-parametric Wilcoxon-Mann-Whitney test (Table SI). Metabolites retained in FFPE were characterized by a lower molecular weight (P=2.20x10^{-16}; FDR=2.64x10^{-15}), polarizability (P=8.32x10^{-9}; FDR=4.99x10^{-8}) and refractivity (P=4.41x10^{-8}; FDR=1.76x10^{-7}), as well as higher solubility (P=2.04x10^{-2}; FDR=3.06x10^{-2}) and pKa (P=2.63x10^{-4}; FDR=5.26x10^{-4}). To perform a comparative analysis between FFPE and OCT-embedded tissues, the study focused on the 206 shared metabolites found in both types of samples. Hierarchical clustering was used to distinguish metabolites significantly different between OCT-embedded and FFPE materials (Fig. 2F).

Exploration of differential metabolites between pancreatic cancer and normal tissues. Distinguishing tumor groups from normal groups in tissue samples is vital for further diagnosis. Using normalized data, PLS-DA was attempted. In anticipation of this, the tumor cohorts were separated from the normal cohorts in the two-dimensional score plots (Fig. 3A).

Analysis was performed to elucidate which metabolites were present in tumor but not normal tissue, and vice versa. Therefore, a Student's t-test was performed, and the FC between tumor and normal groups was calculated for the 206 shared metabolites. The metabolites with significant differences were defined as having an FC>1.5 and P<0.05, respectively. In the volcano diagram shown in Fig. 3B, the red dots represent metabolites with significant differences. Overall, 69 of the 206 total metabolites were significantly different between normal and tumor tissue in OCT-embedded samples; only 23 of 206 metabolites were significantly different in FFPE samples (Fig. 3C; Table SII). Among the different tissue types, 39 were increased in tumor tissue, and 45 were downregulated. Most of these compounds in tumor tissues could be categorized as lipid, amino acids and nucleotides both in OCT-embedded and FFPE samples (Fig. 3D). Using the top 40 common metabolites, normal and tumor tissues were delineated both in OCT-embedded samples and FFPE material (Fig. 3E). A total of 10 metabolites, including N-acetylaspartate, β-hydroxyisovalerate, creatinine and guanosine, were significantly differentially expressed in both OCT-embedded and FFPE tumor samples (Fig. 3C; Table SIII). These candidates included amino acids, lipid, nucleotides, carbohydrate cofactors and vitamins, which showed no significant difference between FFPE and OCT-embedded samples (P>0.05; Tables SI and SIII).

Discovery of shared metabolism pathways in both OCT-embedded and FFPE samples. To investigate the metabolism of metabolites significant differentially expressed between tumor and healthy tissues, pathway analysis was performed. All differential metabolites in OCT-embedded or FFPE samples were selected for analysis. Finally, seven metabolic pathways were identified as meaningful (FDR<0.05; Fig. 4; Table SIV), most of which were involved in amino acid metabolism and production. To find the shared metabolic pathways from these seven metabolic pathways, a filter rule was defined: The compounds in the metabolic pathways should belong to either OCT-embedded groups or FFPE groups. However, only three metabolic pathways, namely purine metabolism (FDR=3.73x10^{-3}), arginine and proline metabolism (FDR=1.07x10^{-2}) and pyrimidine metabolism (FDR=3.67x10^{-2}) were shared between both OCT-embedded and FFPE samples. The compounds involved with the three common pathways were listed in Table SV and can be classified under the amino acid, nucleotide and carbohydrate super-classes. These correspond with the previous analysis, indicating that the three categories were not significantly differently enriched between FFPE and OCT-embedded samples (P>0.05). The same results also appeared in their respective sub-classes.

To explore the latent relationship of the compounds with significant differences involved in the three shared pathways, topologic correlation networks between compounds and gene were constructed using Cytoscape software. The node color was set based on the log2 of fold changes comparison between tumor and normal tissues. From the topologic networks, it was observed that glycine, xanthine and adenine, involved in murine metabolism, were upregulated, and glutamine and

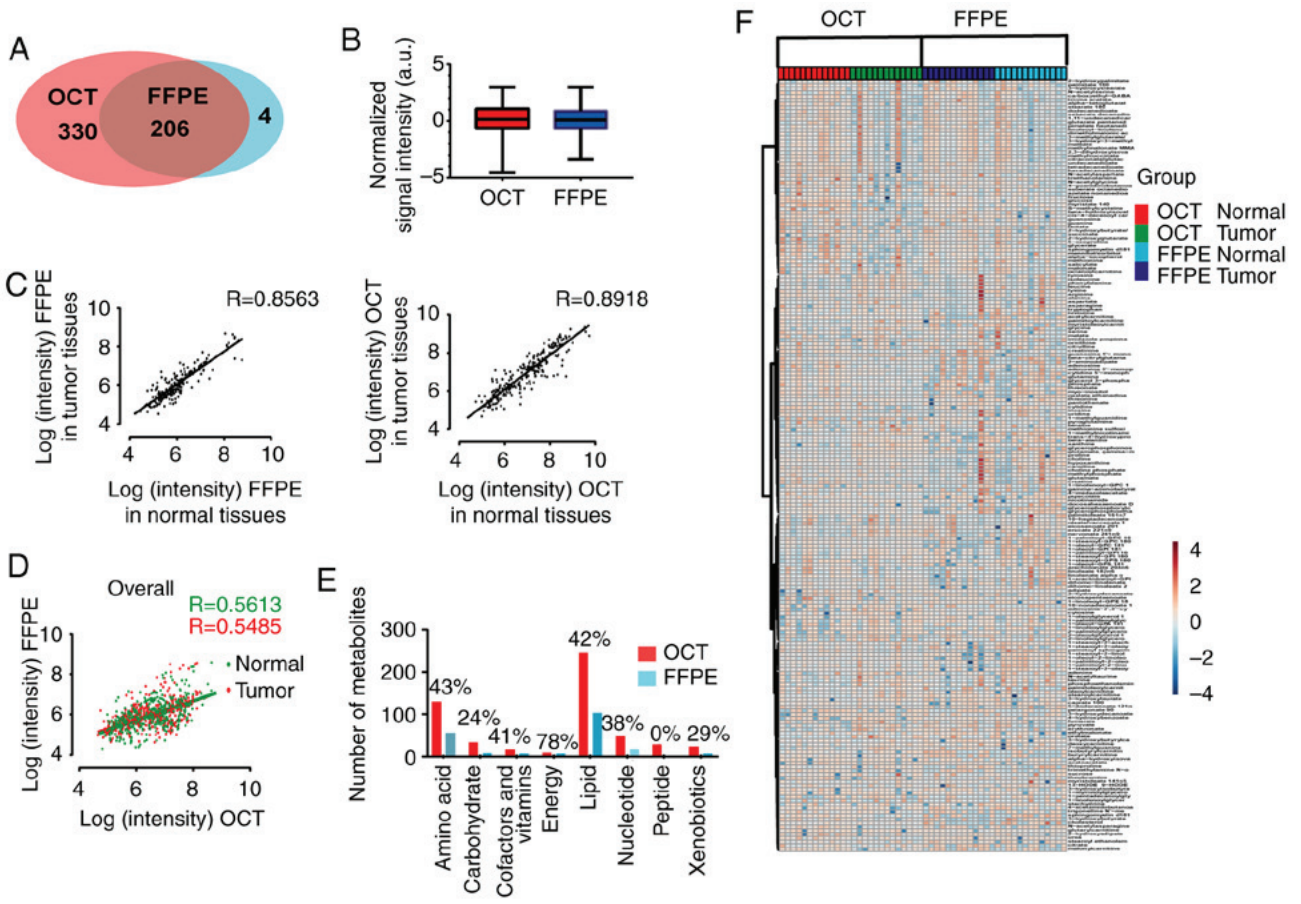

Figure 2. Metabolite detection in FFPE and OCT-embedded samples, and reproducibility and consistency assessment. (A) Venn diagram showing the intersection between OCT-embedded and FFPE metabolomic data in the experimental settings. (B) Box-and-whisker plot representing the relative signal intensity of all metabolites found in OCT-embedded and FFPE tissues. Box plot whiskers extend from the 5 to 95th percentile. (C) Reproducibility plots of detected metabolites in FFPE tissue (left) and OCT-embedded tissue (normal vs. tumor; right), respectively. Pearson correlation analysis was performed to assess correlation coefficients between the intensity of each detected metabolite among the FFPE tissues replicates and OCT-embedded tissues replicates. (D) Correlation plots of detected metabolites between FFPE and OCT-embedded tissues in eight super-classes. Pearson correlation analysis was performed to assess correlation coefficients between the intensity of each detected metabolite between FFPE and OCT-embedded samples. The red plots and green plots represent normal and tumor groups, respectively. (E) Bar plot of the number of metabolites found in OCT-embedded and FFPE samples. The metabolites are categorized according to super-class membership. Bar height refers to amount of metabolites in each super-class preserved in FFPE or OCT-embedded samples. The percentage represents the proportion of the metabolites preserved in the FFPE samples of each class. (F) Heatmap of the 206 metabolites from OCT-embedded and FFPE samples. Hierarchical clustering (Ward method) was used for unsupervised classification. The phenotypic labels of the sample are indicated as a colored band on top of the heatmap. FFPE, formalin-fixed paraffin-embedded; OCT, optimal cutting temperature.

adenosine were downregulated in tumor tissues (Fig. 5A). Proline and *trans*-4-hydroxyproline were increased in arginine and proline metabolism, whereas glutamine, urea and citrulline were significantly decreased in tumor tissues (Fig. 5B). In pyrimidine metabolism, orotate, β-alanine, and cytosine were upregulated; however, certain compounds, such as glutamine, urea and cytidine were downregulated in tumor tissues (Fig. 5C). From the networks, it was also found that an upregulated compound, pyruvate, was involved in the glycolysis and gluconeogenesis metabolism pathway, which was an important downstream target of the arginine and proline metabolism in tumor tissues (Fig. 5D).

Discussion

The past several years has witnessed the development of metabolomics; however, the majority of metabolomics research has been conducted using frozen or fresh tissues. Several studies using FFPE materials and UPLC-MS/MS-based metabolomic profiling have been reported in the study of prostate cancer (36), sarcomas (21) and thyroid cancer (37). These works demonstrated the technical feasibility of using patient FFPE blocks for metabolomic studies. Meanwhile, FFPE materials can be utilized for retrospective studies into biomarker discovery and drug screening (16). For example, studies have identified P53, CD45, human epidermal growth factor receptor 2 and β-actin as biomarkers using tonsil and breast tissue sections from FFPE samples in retrospective studies (13). However, few metabolomic studies have studied pancreatic cancer using FFPE tissue blocks (38-40). These studies primarily aimed to perform metabolic profiling using fresh material, such as cells and urine, but were limited in comparing the metabolic profiles of FFPE tissue blocks and OCT-embedded blocks. In the present study, metabolites extracted from FFPE tissue blocks were comprehensively analyzed compared with those in corresponding OCT-embedded blocks from patients with PDAC. The similarities and differences in class categorization and physical/chemical properties of those detectable

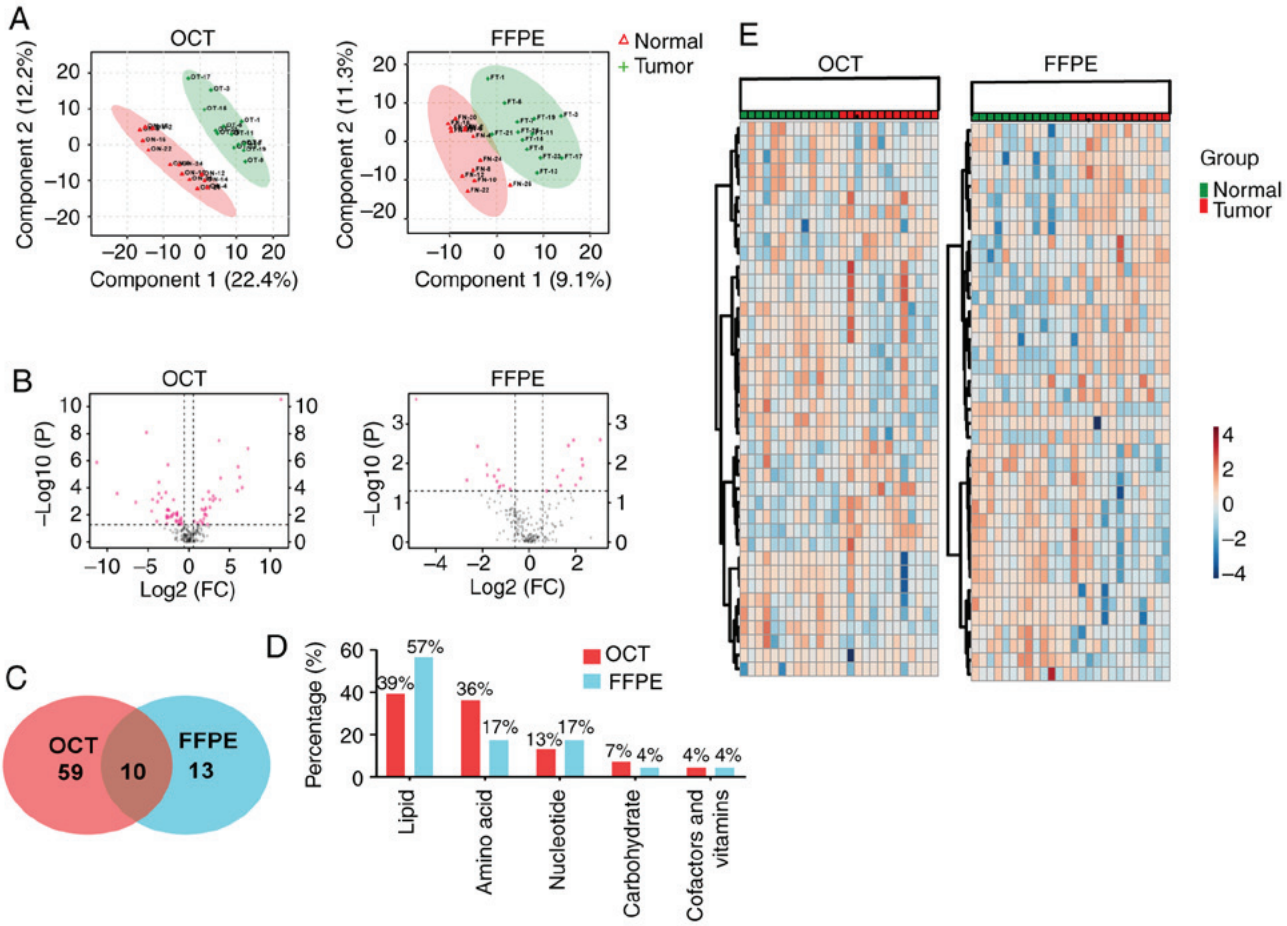

Figure 3. Differentiation between normal and tumor tissue, and exploration of metabolites with significant differences. (A) Two-dimension score plots of tumor and normal samples between the first and second major principal components. The distinct clustering of tumor and normal samples was observed in both the OCT-embedded tissue group (left) and the FFPE tissue group (right). (B) Volcano diagram presenting the differences in metabolites between tumor and normal samples selected with an FC threshold >1.5 and a Student's t-test threshold P<0.05 in OCT-embedded (left) and FFPE (right) tissues. The red dots indicate the metabolites with significant differences. The grey dots indicate the metabolites without significant differences. P-values were transformed by -log10 such that more significant features were plotted higher on the graph. (C) Venn diagram showing the intersection between OCT-embedded and FFPE tissue metabolites with significant differences. (D) Bar plot of the significant differentially abundant metabolites in OCT-embedded and FFPE tumor tissue samples. The metabolites are categorized according to super-class. The percentage above each bar represents the proportion of detectable metabolites for each sample preparation in each super-class. (E) Heatmap of top 40 common metabolites from OCT-embedded (left) and FFPE (right) samples. Hierarchical clustering (Ward method) was used for unsupervised classification. The phenotypic labels of the sample are indicated as a colored band on top of the heatmap. FC, fold change; FFPE, formalin-fixed paraffin-embedded; OCT, optimal cutting temperature.

metabolites from the differentially prepared tissues were characterized. Then, shared and unique metabolic biomarkers and pathways in the two types of tissue blocks were explored, potentially aiding the identification of pathways critical for the metabolism of pancreatic cancer cells.

First, UPLC-MS/MS-based metabolomic profiling was selected for the metabolic analysis. Several studies have confirmed that MS/MS-based platforms, which use hydrophilic interaction LC with positive/negative ion switching, can be compatible with polar metabolites from any biological source, such as FFPE tumor tissue (41,42). Additionally, a high correlation (r>0.80) was found for the 13 replicates of the FFPE and OCT-embedded samples, demonstrating the feasibility of the method. Furthermore, the tight correlation between OCT-embedded and FFPE samples, both overall and for the majority of super-classes, suggested that there was minimal technical variability across runs. These results indicated that measurements of metabolite content in FFPE tissues may be applicable for further metabolite analysis.

To compare metabolic data from OCT-embedded and FFPE tissue samples, a comprehensive characterization of the categorization of metabolites in FFPE and OCT-embedded samples was performed. A previous study used the composition ratio to compare the categorization of metabolites in FFPE and OCT-embedded samples (43). Overall, 38.4% of compounds were preserved in human tumor FFPE specimens compared with their paired frozen counterparts; however, the properties of retained metabolites varied notably across class categories. Certain super-classes of metabolites, including xenobiotics, energy, carbohydrates, cofactors, vitamins and amino acids, were reported have to no significant difference between FFPE and OCT-embedded samples in prostate cancer (27). In the present study, it was revealed that the majority of super-classes (nucleotides, cofactors and vitamins, xenobiotics, amino acids, lipid and carbohydrate, and energy) of metabolites detected in OCT-embedded samples could also be identified in FFPE tissue blocks; however, peptides were not. Additionally, certain similarities in the physical/chemical properties of detectable

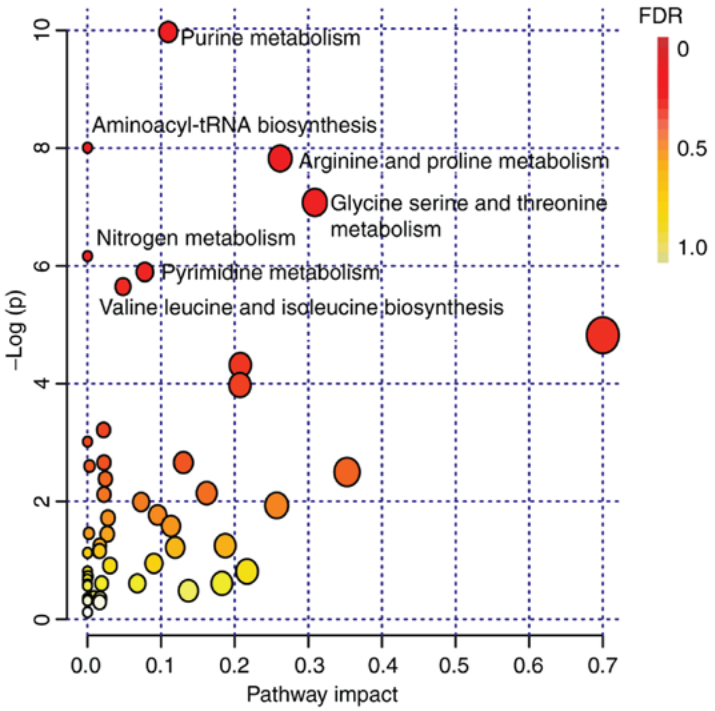

Figure 4. Significant pathways identified in both formalin-fixed paraffin-embedded and optimal cutting temperature-embedded tumor samples. The metabolome view shows all matched pathways according to the P-values from the pathway enrichment analysis and pathway impact values from the pathway topology analysis. Significant pathways are named in the figure.

metabolites were identified, including logP, pKa (strongest base), physiological charge and formal charge. Our findings were similar to a previous report on prostate tissues (27), but it also presented with difference in some aspects, including the sub-classes, which metabolites preserved in. It may be ascribed to a particular cancer tissue type and were susceptible to FFPE processing.

Pancreatic cancer is one of the most lethal cancers in the world, with low survival and poor prognosis (5). Several metabolomic studies have led to an enhanced understanding of disease mechanisms, and the discovery of novel diagnostic biomarkers (44,45). In the present study, it was found that 69 metabolites showed significant differences in OCT-embedded groups, and 23 metabolites were significantly different in FFPE groups. Concerning their categories, most metabolites could be classified as lipids, amino acids and nucleotides, which were altered in tumor tissue. Similarly, it was identified that metabolites belonged to peptide, nucleotide, amino acid and lipid-related super-classes were dysregulated in human cancer in previous study (46). In this study, we found that the majority of metabolites associated with amino acids and lipids were perturbed in tumor tissues both in OCT-embedded and FFPE samples. This finding was consistent with previous studies showing that amino acid and lipid metabolism were involved in several tumorigenic processes (47-50). For example, tryptophan metabolism is recognized as a microenvironmental factor for suppressing antitumor responses (7), and tryptophan was found to be dysregulated in PDAC (51). Of the metabolites identified in the present study, 10 were identified as significantly differentially expressed in tumor tissue in both the OCT-embedded and FFPE groups. Consistent with previous studies (21,27), the classification of compounds which were preserved in FFPE specimens were amino acids, carbohydrates, lipids, nucleotides, cofactors and vitamins. Recently, research regarding the metabolic profiling of pancreatic cancer using various types of biological materials has been reported (8). These reports suggested several potential biomarkers of pancreatic cancer, such as alanine, creatine, 3-hydroxybutyrate, 3-hydroxyisovalerate, glucose, asparagine and proline (17,18). Most of them were involved in amino acid metabolic pathways, such as alanine and aspartate metabolism, arginine and proline metabolism, and tryptophan metabolism (46,51). Of note, 10 metabolites were found to be altered in tumor tissues in the present study. Among them, N-acetylaspartate and creatinine have been reported to be critical for cancer metabolism. N-acetylaspartate was associated with autophagy and histone acetylation in non-small cell lung cancer and impacted cell survival (52,53). Creatine, a diagnostic indicator of prostate cancer, was shown to be a marker of high mortality in numerous cancers, such as prostate, gastrointestinal and prostate cancer (54-56). Thus, creatine may be a candidate biomarker of malignant pancreatic cancer.

Through KEGG pathway enrichment analysis, it was found that three metabolic pathways (purine metabolism, arginine/proline metabolism and pyrimidine metabolism) were markedly altered in both OCT-embedded and FFPE samples. The proline pathway was linked with hypoxia in pancreatic cancer and triggered a hypoxic stress response (57). The metabolism of proline as a stress substrate modulates the carcinogenic pathway, and is responsible for destroying intracellular reactive oxygen species, mediated via p53-induced proline oxidase (57-59). A previous study reported that increased levels of proline and *trans*-4-hydroxyproline in

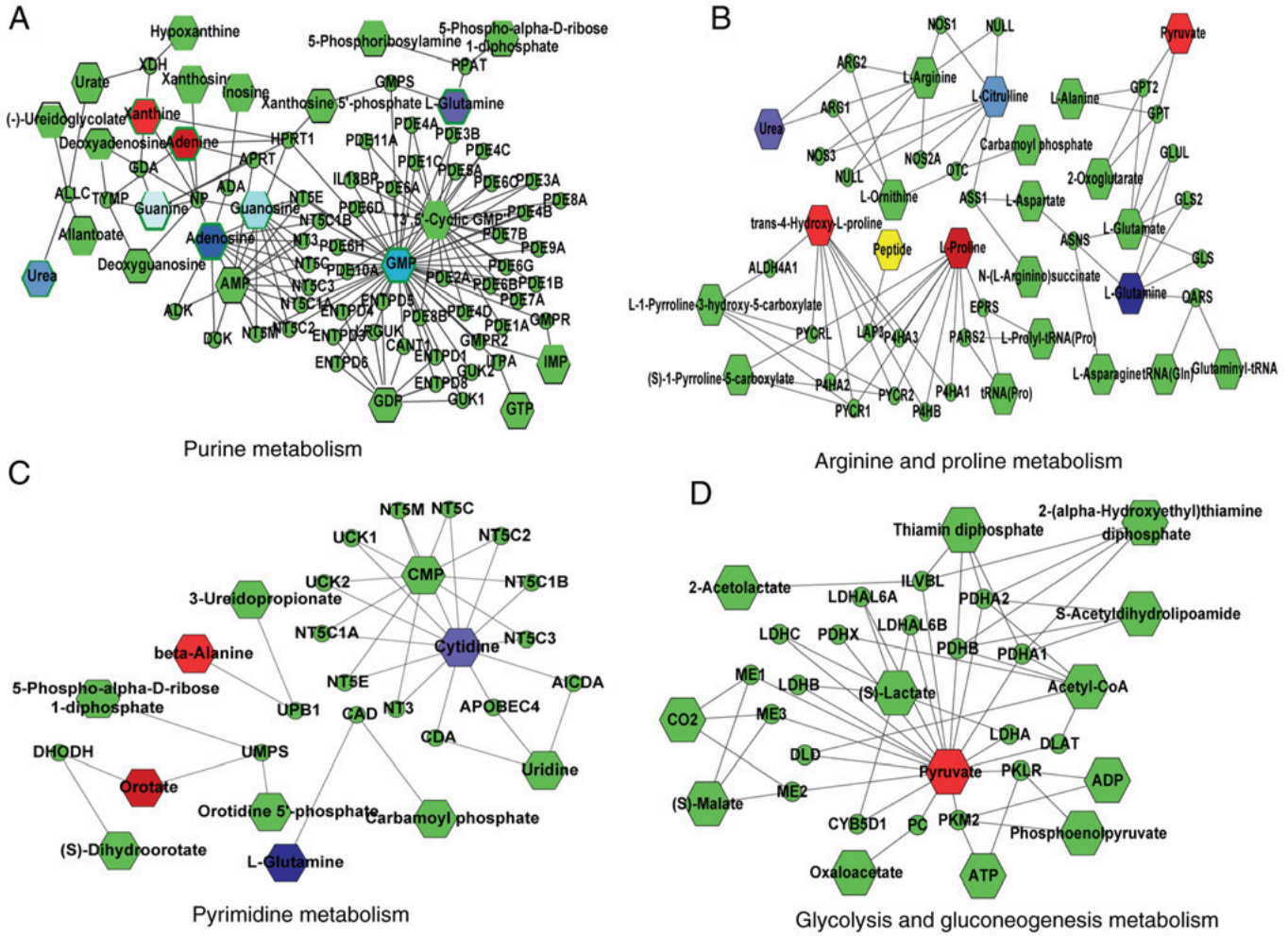

Figure 5. Discovery of metabolic pathway identified in both optimal cutting temperature-embedded and formalin-fixed paraffin-embedded samples. Topology networks of (A) purine metabolism pathway, (B) proline metabolism pathway, (C) pyrimidine metabolism pathway and (D) glycolysis and gluconeogenesis pathway illustrated by Cytoscape software. Circles represent genes and hexagons represent metabolites. Gradient from red to purple indicates the up- or downregulation of the metabolites.

tumor tissues, in part, are due to an alteration of intracellular redox status and ultimately affect the biosynthesis of nucleic acid and fatty acids (57). The pathway analysis also revealed the significance of the purine metabolic pathway, which plays an important role in providing cellular energy, and indicates cancer cell survival and proliferation (60,61). In addition, pyrimidine metabolism, which is a key metabolic bottleneck important for DNA replication in tumor cells, and a valuable diagnostic and therapeutic target, was disrupted in tumor tissues (62,63). Furthermore, the compounds involved in the three shared pathways could be classified into the amino acid, nucleotide and carbohydrate super-classes. These metabolites were demonstrated to be preserved similarly in FFPE and OCT-embedded samples. From the latent network of the compounds built by Cytoscape software, the glycolysis and gluconeogenesis metabolic pathways were latent and downstream of the arginine and proline metabolism pathway. This finding was consistent with a previous study that pancreatic cancer was associated with the 'Warburg effect' (14), which is commonly referred to as 'aerobic glycolysis'. Collectively, these results are consistent with the existing cancer literature and illustrate that potential metabolic pathways in cancer biology can be analyzed in FFPE tissue blocks using UPLC-MS/MS.

However, there were certain limitations to the present study. The number of patients was small compared with other metabolomic studies of pancreatic cancer tissues. However, the major purpose of this study was to investigate the feasibility of employing FFPE tissue samples for the metabolomic studies of human pancreatic cancer tissue, and to identify differences between FFPE and OCT-embedded specimens. Based on the present findings, future studies may further explore the metabolic profiling of patients with pancreatic cancer. Furthermore, using categories of the compounds to calculate the composition ratio analysis for metabolites may not be sufficient to represent the specific properties of metabolites. Thus, the physical/chemical properties of the detectable compounds, and the different metabolites and potential metabolic pathways altered in pancreatic tumors also require further analysis in both FFPE and OCT-embedded specimens.

In conclusion, this study focused on the application of UPLC-MS/MS-based metabolic profiling of FFPE and OCT-embedded pancreatic tissues in the discovery and comparison of candidate biomarkers and potential metabolic pathways

altered in pancreatic tumors to distinguish tumor and normal tissues. A total of 10 metabolites, including N-acetylaspartate, β-hydroxyisovalerate, creatinine and guanosine, may be potential candidate biomarkers of malignant pancreatic tissue samples. It was also found that three metabolic pathways, namely purine metabolism, arginine/proline metabolism and pyrimidine metabolism, were significantly altered in both OCT-embedded and FFPE samples. The present findings suggested that FFPE specimens may provide similarly reliable metabolic data as OCT-embedded specimens for PDAC, and may be utilized in further diagnostic and retrospective studies into metabolic biomarkers and pathways.

Acknowledgements

We sincerely appreciate Dr Michael C. Lin (360 Scientific Consulting) for his advice and assistance with the language consulting of the manuscript.

Funding

The present study was supported by THE National Natural Science Foundation of China (grant nos. 81673607, 81303235, 81774011 and 81473434), Natural Science Foundation of Zhejiang Province (grant no. LY19H280001), Beijing Municipal Natural Science Foundation (grant no. 7152140), Beijing Nova Program (grant no. XXJH2015B098) and rgw Science and Technology Research Project for Public Welfare in Huzhou (grant no. 2019GZ24).

Availability of data and materials

The analyzed data sets generated during the present study are available from the corresponding author on reasonable request.

Authors' contributions

All authors made substantial contributions to the conception and design of the study. MCG and YS are the grant holders, initiated the study, and participated in its design and coordination. DF, XZ, and YLW were responsible for protocol design, statistical analysis and manuscript drafting. JY, LL and YFQ contributed to the collection and embedding of clinical samples, and the extraction of metabolic data. QL and LPC contributed to revising the manuscript. All authors read and approved the final manuscript.

Ethics approval and consent to participate

The study was approved by the Institutional Review Board of Chinese PLA General Hospital. Informed consent was obtained from all individual participants in the study.

Patient consent for publication

Not applicable.

Competing interests

The authors declare that they have no competing interests.

References

1. Suzuki K, Takeuchi O, Suzuki Y and Kitagawa Y: Mechanisms of metformin's anti-tumor activity against gemcitabine-resistant pancreatic adenocarcinoma. Int J Oncol 54: 764-772, 2019.
2. Wei DM, Jiang MT, Lin P, Yang H, Dang YW, Yu Q, Liao DY, Luo DZ and Chen G: Potential ceRNA networks involved in autophagy suppression of pancreatic cancer caused by chloroquine diphosphate: A study based on differentially-expressed circRNAs, lncRNAs, miRNAs and mRNAs. Int J Oncol 54: 600-626, 2019.
3. Lin QJ, Yang F, Jin C and Fu DL: Current status and progress of pancreatic cancer in China. World J Gastroenterol 21: 7988-8003, 2015.
4. Son J, Lyssiotis CA, Ying H, Wang X, Hua S, Ligorio M, Perera RM, Ferrone CR, Mullarky E, Shyh-Chang N, *et al*: Glutamine supports pancreatic cancer growth through a KRAS-regulated metabolic pathway. Nature 496: 101-105, 2013.
5. Huang Q, Tan Y, Yin P, Ye G, Gao P, Lu X, Wang H and Xu G: Metabolic characterization of hepatocellular carcinoma using nontargeted tissue metabolomics. Cancer Res 73: 4992-5002, 2013.
6. Keum N, Yuan C, Nishihara R, Zoltick E, Hamada T, Martinez Fernandez A, Zhang X, Hanyuda A, Liu L, Kosumi K, *et al*: Dietary glycemic and insulin scores and colorectal cancer survival by tumor molecular biomarkers. Int J Cancer 140: 2648-2656, 2017.
7. McDonnell SR, Hwang SR, Rolland D, Murga-Zamalloa C, Basrur V, Conlon KP, Fermin D, Wolfe T, Raskind A, Ruan C, *et al*: Integrated phosphoproteomic and metabolomic profiling reveals NPM-ALK-mediated phosphorylation of PKM2 and metabolic reprogramming in anaplastic large cell lymphoma. Blood 122: 958-968, 2013.
8. Vernieri C, Pusceddu S, Fucà G, Indelicato P, Centonze G, Castagnoli L, Ferrari E, Ajazi A, Pupa S, Casola S, *et al*: Impact of systemic and tumor lipid metabolism on everolimus efficacy in advanced pancreatic neuroendocrine tumors (pNETs). Int J Cancer 144: 1704-1712, 2019.
9. Cacciatore S, Hu X, Viertler C, Kap M, Bernhardt GA, Mischinger HJ, Riegman P, Zatloukal K, Luchinat C and Turano P: Effects of intra- and post-operative ischemia on the metabolic profile of clinical liver tissue specimens monitored by NMR. J Proteome Res 12: 5723-5729, 2013.
10. Priolo C, Pyne S, Rose J, Regan ER, Zadra G, Photopoulos C, Cacciatore S, Schultz D, Scaglia N, McDunn J, *et al*: AKT1 and MYC induce distinctive metabolic fingerprints in human prostate cancer. Cancer Res 74: 7198-7204, 2014.
11. Liu L, Tabung FK, Zhang XH, Nowak JA, Qian ZR, Hamada T, Nevo D, Bullman S, Mima K, Kosumi K, *et al*: Diets that promote colon inflammation associate with risk of colorectal carcinomas that contain fusobacterium nucleatum. Clin Gastroenterol Hepatol 16: 1622-1631.e3, 2018.
12. Ruan J, Zheng H, Rong X, Zhang J, Fang W, Zhao P and Luo R: Over-expression of cathepsin B in hepatocellular carcinomas predicts poor prognosis of HCC patients. Mol Cancer 15: 17, 2016.
13. Cors JF, Kashyap A, Fomitcheva Khartchenko A, Schraml P and Kaigala GV: Tissue lithography: Microscale dewaxing to enable retrospective studies on formalin-fixed paraffin-embedded (FFPE) tissue sections. PLoS One 12: e0176691, 2017.
14. Warburg O: On the origin of cancer cells. Science 123: 309-314, 1956.
15. Mayer A, Schmidt M, Seeger A, Serras AF, Vaupel P and Schmidberger H: GLUT-1 expression is largely unrelated to both hypoxia and the warburg phenotype in squamous cell carcinomas of the vulva. BMC Cancer 14: 760, 2014.
16. Poste G: Bring on the biomarkers. Nature 469: 156-157, 2011.
17. Fang F, He X, Deng H, Chen Q, Lu J, Spraul M and Yu Y: Discrimination of metabolic profiles of pancreatic cancer from chronic pancreatitis by high-resolution magic angle spinning 1H nuclear magnetic resonance and principal components analysis. Cancer Sci 98: 1678-1682, 2007.
18. Kaplan O, Kushnir T, Askenazy N, Knubovets T and Navon G: Role of nuclear magnetic resonance spectroscopy (MRS) in cancer diagnosis and treatment: 31P, 23Na, and 1H MRS studies of three models of pancreatic cancer. Cancer Res 57: 1452-1459, 1997.
19. Buck A, Ly A, Balluff B, Sun N, Gorzolka K, Feuchtinger A, Janssen KP, Kuppen PJ, van de Velde CJ, Weirich G, *et al*: High-resolution MALDI-FT-ICR MS imaging for the analysis of metabolites from formalin-fixed, paraffin-embedded clinical tissue samples. J Pathol 237: 123-132, 2015.

20. Wang H, Wang L, Zhang H, Deng P, Chen J, Zhou B, Hu J, Zou J, Lu W, Xiang P, *et al*: H-1 NMR-based metabolic profiling of human rectal cancer tissue. Mol Cancer 12: 121, 2013.
21. Kelly AD, Breitkopf SB, Yuan M, Goldsmith J, Spentzos D and Asara JM: Metabolomic profiling from formalin-fixed, paraffin-embedded tumor tissue using targeted LC/MS/MS: Application in sarcoma. PLoS One 6: e25357, 2011.
22. Aimetti M, Cacciatore S, Graziano A and Tenori L: Metabonomic analysis of saliva reveals generalized chronic periodontitis signature. Metabolomics 8: 465-474, 2012.
23. Lim J, Kim Y, Lee W, Kim M, Lee EJ, Kang CS and Han K: Fresh-frozen, optimal cutting temperature (OCT) compound-embedded bone marrow aspirates: A reliable resource for morphological, immunohistochemical and molecular examinations. Int J Laboratory Hematol 32: e34-39, 2010.
24. Liu M, Zhao SQ, Yang L, Li X, Song X, Zheng Y, Fan J and Shi H: A direct immunohistochemistry (IHC) method improves the intraoperative diagnosis of breast papillary lesions including breast cancer. Discov Med 28: 29-37, 2019.
25. Evans AM, DeHaven CD, Barrett T, Mitchell M and Milgram E: Integrated, nontargeted ultrahigh performance liquid chromatography/electrospray ionization tandem mass spectrometry platform for the identification and relative quantification of the small-molecule complement of biological systems. Anal Chem 81: 6656-6667, 2009.
26. Yuan M, Breitkopf SB, Yang X and Asara JM: A positive/negative ion-switching, targeted mass spectrometry-based metabolomics platform for bodily fluids, cells, and fresh and fixed tissue. Nat Protoc 7: 872-881, 2012.
27. Cacciatore S, Zadra G, Bango C, Penney KL, Tyekucheva S, Yanes O and Loda M: Metabolic profiling in formalin-fixed and paraffin-embedded prostate cancer tissues. Mol Cancer Res 15: 439-447, 2017.
28. Li CF, Tsai HH, Ko CY, Pan YC, Yen CJ, Lai HY, Yuh CH, Wu WC and Wang JM: HMDB and 5-AzadC combination reverses tumor suppressor CCAAT/enhancer-binding protein delta to strengthen the death of liver cancer cells. Mol Cancer Ther 14: 2623-2633, 2015.
29. Wishart DS, Feunang YD, Marcu A, Guo AC, Liang K, Vázquez-Fresno R, Sajed T, Johnson D, Li C, Karu N, *et al*: HMDB 4.0: The human metabolome database for 2018. Nucleic Acids Res 46: D608-D617, 2018.
30. Xia J, Psychogios N, Young N and Wishart DS: MetaboAnalyst: A web server for metabolomic data analysis and interpretation. Nucleic Acids Res 37: W652-W660, 2009.
31. Xia J and Wishart DS: Web-based inference of biological patterns, functions and pathways from metabolomic data using MetaboAnalyst. Nat Protoc 6: 743-760, 2011.
32. Villanueva RAM and Chen ZJ: ggplot2: Elegant graphics for data analysis (2nd ed.). Meas Interdisciplinary Res Perspect 17: 160-167, 2019.
33. Benjamini Y and Hocherg Y: Controlling the false discovery rate: A practical and powerful approach to multiple testing. J Royal Stat Soc Series B (Methodological) 57: 289-300, 1995.
34. Gao J, Tarcea VG, Karnovsky A, Mirel BR, Weymouth TE, Beecher CW, Cavalcoli JD, Athey BD, Omenn GS, Burant CF and Jagadish HV: Metscape: A Cytoscape plug-in for visualizing and interpreting metabolomic data in the context of human metabolic networks. Bioinformatics 26: 971-973, 2010.
35. Shannon P, Markiel A, Ozier O, Baliga NS, Wang JT, Ramage D, Amin N, Schwikowski B and Ideker T: Cytoscape: A software environment for integrated models of biomolecular interaction networks. Genome Res 13: 2498-2504, 2003.
36. Putluri N, Shojaie A, Vasu VT, Nalluri S, Vareed SK, Putluri V, Vivekanandan-Giri A, Byun J, Pennathur S, Sana TR, *et al*: Metabolomic profiling reveals a role for androgen in activating amino acid metabolism and methylation in prostate cancer cells. PLoS One 6: e21417, 2011.
37. Wojakowska A, Chekan M, Marczak Ł, Polanski K, Lange D, Pietrowska M and Widlak P: Detection of metabolites discriminating subtypes of thyroid cancer: Molecular profiling of FFPE samples using the GC/MS approach. Mol Cell Endocrinol 417: 149-157, 2015.
38. Mayers JR, Wu C, Clish CB, Kraft P, Torrence ME, Fiske BP, Yuan C, Bao Y, Townsend MK, Tworoger SS, *et al*: Elevation of circulating branched-chain amino acids is an early event in human pancreatic adenocarcinoma development. Nat Med 20: 1193-1198, 2014.
39. Sadanandam A, Wullschleger S, Lyssiotis CA, Grötzinger C, Barbi S, Bersani S, Körner J, Wafy I, Mafficini A, Lawlor RT, *et al*: A cross-species analysis in pancreatic neuroendocrine tumors reveals molecular subtypes with distinctive clinical, metastatic, developmental, and metabolic characteristics. Cancer Discov 5: 1296-1313, 2015.
40. Nie S, Lo A, Wu J, Zhu J, Tan Z, Simeone DM, Anderson MA, Shedden KA, Ruffin MT and Lubman DM: Glycoprotein biomarker panel for pancreatic cancer discovered by quantitative proteomics analysis. J Proteome Res 13: 1873-1884, 2014.
41. Wojakowska A, Marczak Ł, Jelonek K, Polanski K, Widlak P and Pietrowska M: An optimized method of metabolite extraction from formalin-fixed paraffin-embedded tissue for GC/MS analysis. PLoS One 10: e0136902, 2015.
42. Gika H, Virgiliou C, Theodoridis G, Plumb RS and Wilson ID: Untargeted LC/MS-based metabolic phenotyping (metabonomics/metabolomics): The state of the art. J Chromatogr B Analyt Technol Biomed Life Sci 1117: 136-147, 2019.
43. Kaushik AK, Vareed SK, Basu S, Putluri V, Putluri N, Panzitt K, Brennan CA, Chinnaiyan AM, Vergara IA, Erho N, *et al*: Metabolomic profiling identifies biochemical pathways associated with castration-resistant prostate cancer. J Proteome Res 13: 1088-1100, 2014.
44. DeMarshall C, Goldwaser EL, Sarkar A, Godsey GA, Acharya NK, Thayasivam U, Belinka BA and Nagele RG: Autoantibodies as diagnostic biomarkers for the detection and subtyping of multiple sclerosis. J Neuroimmunol 309: 51-57, 2017.
45. Yokom DW, Stewart J, Alimohamed NS, Winquist E, Berry S, Hubay S, Lattouf JB, Leonard H, Girolametto C, Saad F and Sridhar SS: Prognostic and predictive clinical factors in patients with metastatic castration-resistant prostate cancer treated with cabazitaxel. Can Urol Assoc J 12: E365-E372, 2018.
46. Moreno P, Jiménez-Jiménez C, Garrido-Rodríguez M, Calderón-Santiago M, Molina S, Lara-Chica M, Priego-Capote F, Salvatierra Á, Muñoz E and Calzado MA: Metabolomic profiling of human lung tumor tissues-nucleotide metabolism as a candidate for therapeutic interventions and biomarkers. Mol Oncol 12: 1778-1796, 2018.
47. Zhang J, Pavlova NN and Thompson CB: Cancer cell metabolism: The essential role of the nonessential amino acid, glutamine. EMBO J 36: 1302-1315, 2017.
48. Koutsioumpa M, Hatziapostolou M, Polytarchou C, Mahurkar-Joshi S and Iliopoulos D: H3K4me3 affects glucose metabolism and lipid content in pancreatic cancer. Gastroenterology 152: S115, 2017.
49. Sunami Y, Rebelo A and Kleeff J: Lipid metabolism and lipid droplets in pancreatic cancer and stellate cells. Cancers (Basel) 10: E3, 2017.
50. Krishnamurthy RV, Suryawanshi YR and Essani K: Nitrogen isotopes provide clues to amino acid metabolism in human colorectal cancer cells. Sci Rep 7: 2562, 2017.
51. Jiao L, Maity S, Coarfa C, Rajapakshe K, Chen L, Jin F, Putluri V, Tinker LF, Mo Q, Chen F, *et al*: A prospective targeted serum metabolomics study of pancreatic cancer in postmenopausal women. Cancer Prev Res (Phila) 12: 237-246, 2019.
52. Bogner-Strauss JG: N-acetylaspartate metabolism outside the brain: Lipogenesis, histone acetylation, and cancer. Front Endocrinol (Lausanne) 8: 240, 2017.
53. Lou TF, Sethuraman D, Dospoy P, Srivastva P, Kim HS, Kim J, Ma X, Chen PH, Huffman KE, Frink RE, *et al*: Cancer-Specific Production of N-Acetylaspartate via NAT8L Overexpression in Non-Small Cell Lung Cancer and Its Potential as a Circulating Biomarker. Cancer Prev Res (Phila) 9: 43-52, 2016.
54. Wang M, Zou L, Liang J, Wang X, Zhang D, Fang Y, Zhang J, Xiao F and Liu M: The urinary sarcosine/creatinine ratio is a potential diagnostic and prognostic marker in prostate cancer. Med Sci Monit 24: 3034-3041, 2018.
55. Lin HL, Chen CW, Lu CY, Sun LC, Shih YL, Chuang JF, Huang YH, Sheen MC and Wang JY: High preoperative ratio of blood urea nitrogen to creatinine increased mortality in gastrointestinal cancer patients who developed postoperative enteric fistulas. Kaohsiung J Med Sci 28: 418-422, 2012.
56. Weinstein SJ, Mackrain K, Stolzenberg-Solomon RZ, Selhub J, Virtamo J and Albanes D: Serum creatinine and prostate cancer risk in a prospective study. Cancer Epidemiol Biomarkers Prev 18: 2643-2649, 2009.
57. Phang JM, Donald SP, Pandhare J and Liu Y: The metabolism of proline, a stress substrate, modulates carcinogenic pathways. Amino Acids 35: 681-690, 2008.

58. Eales KL, Hollinshead KE and Tennant DA: Hypoxia and metabolic adaptation of cancer cells. Oncogenesis 5: e190, 2016.
59. Tang L, Zeng J, Geng P, Fang C, Wang Y, Sun M, Wang C, Wang J, Yin P, Hu C, *et al*: Global metabolic profiling identifies a pivotal role of proline and hydroxyproline metabolism in supporting hypoxic response in hepatocellular carcinoma. Clin Cancer Res 24: 474-485, 2018.
60. Karigane D, Kobayashi H, Morikawa T, Ootomo Y, Sakai M, Nagamatsu G, Kubota Y, Goda N, Matsumoto M, Nishimura EK, *et al*: p38α activates purine metabolism to initiate hematopoietic stem/progenitor cell cycling in response to stress. Cell Stem Cell 19: 192-204, 2016.
61. Matsuyama M, Wakui M, Monnai M, Mizushima T, Nishime C, Kawai K, Ohmura M, Suemizu H, Hishiki T, Suematsu M, *et al*: Reduced CD73 expression and its association with altered purine nucleotide metabolism in colorectal cancer cells robustly causing liver metastases. Oncol Lett 1: 431-436, 2010.
62. El Kouni MH: Pyrimidine metabolism in schistosomes: A comparison with other parasites and the search for potential chemotherapeutic targets. Comp Biochem Physiol B Biochem Mol Biol 213: 55-80, 2017.
63. Ser Z, Gao X, Johnson C, Mehrmohamadi M, Liu X, Li S and Locasale JW: Targeting one carbon metabolism with an antimetabolite disrupts pyrimidine homeostasis and induces nucleotide overflow. Cell Rep 15: 2367-2376, 2016.